Appl Magn Reson (2012) 43:321–330
DOI 10.1007/s00723-012-0371-4

Applied
Magnetic Resonance

Functional Magnetic Resonance Imaging Data Analysis by Autoregressive Estimator

Hernán Cervantes · Carlos A. C. Jousseph · Said R. Rabbani

Received: 14 September 2011 / Published online: 29 June 2012

Abstract The autoregressive (AR) estimator, a non-parametric method, is used to analyze functional magnetic resonance imaging (fMRI) data. The same method has been used, with success, in several other time series data analysis. It uses exclusively the available experimental data points to estimate the most plausible power spectra compatible with the experimental data and there is no need to make any assumption about non-measured points. The time series, obtained from fMRI block paradigm data, is analyzed by the AR method to determine the brain active regions involved in the processing of a given stimulus. This method is considerably more reliable than the fast Fourier transform or the parametric methods. The time series corresponding to each image pixel is analyzed using the AR estimator and the corresponding poles are obtained. The pole distribution gives the shape of power spectra, and the pixels with poles at the stimulation frequency are considered as the active regions. The method was applied in simulated and real data, its superiority is shown by the receiver operating characteristic curves which were obtained using the simulated data.

1 Introduction

Functional magnetic resonance imaging (fMRI) is one of the most interesting and active research areas in brain mapping. It can be used to trace the brain activity in vivo in a non-invasive way with millimetric spacial resolution, [1–4]. The change in signal intensity caused by the variation of concentration of oxy and deoxyhemoglobin due to the oxygen consumption by the active neurons is relatively small, and

H. Cervantes (✉) · S. R. Rabbani
Departamento de Física Geral, Instituto de Física, Universidade de São Paulo,
Rua do Matão, Travessa R 187, Caixa Postal 66318, São Paulo, SP CEP 05315-970, Brazil
e-mail: hernan@if.usp.br

C. A. C. Jousseph
Universidade Tecnológica Federal do Paraná, Medianeira, PR, Brazil

difficult to be determined. There are already a variety of techniques [4, 5], and continuously new ones are being proposed to analyze the perfusion-based, flow-based or susceptibility contrast-based fMRI signal. Each one presenting some advantages and shortcomings. The method proposed in this article has the advantage that only the measured points are used, there is no need to assume any specific hemodynamic response function (hrf) and the values of the time series can be real or complex numbers.

Since the series corresponding to the temporal evolution of active pixels in a fMRI block paradigm signal contains a weak periodic component, it could be Fourier transformed to obtain the spectra. The presence of a component at stimulation frequency can be used to distinguish the active from non-active pixels. However, due to poor signal-to-noise ratio and scarcity of experimental data points, the spectra obtained by fast Fourier transform (FFT) are very noisy and full of artifacts making it impossible to single out the feeble periodic component present in active pixels. Lange and Zeger [6] suggested a fMRI data analysis method using the discrete FT to calculate the power spectrum in the neighborhood of stimulus frequency and their harmonics. But, their method stands in stark contrast with ours in several aspects: (a) it is a parametric one, (b) they assumed that the fMRI signal is a convolution of the known stimulus function with one unobservable, unknown and yet spatially variable hrf, supposed to be in a class of parametric functions whose FT can be evaluated analytically, or whose partial derivatives have FT that can be evaluated analytically. Lange and Zeger's method does a frequency domain regression with hundreds of whole head images. Marchini and Ripley [7] use the FFT after de-trend, hard noise filtering and zero padding. In this work, no pre-processing is needed.

The AR estimator used in this paper has been used in a variety of problems with excellent results; the AR estimator uses exclusively the available experimental data points to estimate the most plausible power spectra compatible with the experimental data [8–11].

The periodic stimulation of a subject in fMRI experiment, using block paradigm, produces physiological changes in the brain region responsible for the processing of these stimulus. These changes affect the nuclear magnetic resonance (NMR) signal in a feeble way [2, 12–14]. A series of images are obtained during the active and rest periods at regular time intervals producing a minute periodic component in the time series corresponding to the active pixels. Often a post-processing is needed to realign, normalize and correct eventual movements. Also, a local spatial mean can be obtained to increase the harmonic signals and avoid isolated false positives. Due to the background signal, the periodic component in the time series is almost imperceptible and needs further treatment to single it out.

The power spectra obtained by FT invariably present a windowing artifact. Windowing is, in fact, an artificial constraint imposed on experimental data, by assuming null values for data points outside the measurement interval which results in a convolution of the real spectra and the window, which leads to a distorted spectra. In order to obtain the spectra as accurate as possible, no restrain should be imposed on the information outside the observation period. Since the fMRI block paradigm time series contain noise, it can be divided into two parts: a casual part and a stochastic one. The causal part can be modeled analytically by some function

(in general unknown) and the second part is a random series. The AR estimator models the casual part using the past data to predict the future one. In order to use the AR estimator, the time series must be stationary, roughly speaking, it means that the causal part should be oscillatory. If the time series causal part has a small time variation, a quasi-stationary time series, the AR estimator can still be used. Often the AR process is used in fMRI data analysis to remove "T1 effects" that arose from the spin–lattice relaxation [15].

The AR estimator can also be applied to complex numbers. In the case of fMRI data, it is possible to construct the time series using the real and imaginary parts of the reconstructed images rather than the pixel module. The use of complex numbers instead of pixel modulus ensures that the noise characteristic remains unchanged [16]. Using this method with fMRI block paradigm it is possible to determine the region of the brain involved for the processing of a given stimulus. By AR modeling of the time series of each pixel a frequency decomposition is achieved. Pixels with peak at the stimulus frequency or close to it will be considered active pixels, otherwise, are inactive ones. As the AR model uses past values to calculate the future values plus noise it is possible, in principle, to extend the time signal and, by averaging, build the hrf curve in each active pixel.

In order to measure the method performance, receiver operating characteristic (ROC) curves was built. ROC curves show the sensitivity, as the fraction of correctly classified active pixels, against the specificity, weighed by the fraction of incorrectly classified inactive pixels.

2 Materials and Methods

2.1 Autoregressive Method

There are several methods for analysis of the time series with limited experimental data and/or low signal-to-noise ratio. One of these methods is the AR estimator, a robust estimator, which uses the preceding data points to predict the following ones [8–11]. The time series is considered as a function corrupted by white noise, where each term is modeled as a linear combination of p previous terms plus noise (Eq. 1). The coefficients, a_m, $m = 1, \ldots, p$, are determined from the recorded values of the time series. The value of p, which is used to determine the following points is normally a critical input parameter.

The AR estimator can also be defined as an output of a filter driven by a white noise:

$$s_t = -\sum_{m=1}^{p} a_m s_{t-m} + \epsilon_t, \tag{1}$$

where s_t is the time series term at time t, the a_m's are the filter coefficients, p is the filter order and ϵ_t is a zero mean white noise process. The corresponding spectrum can be obtained by the application of the FT to Eq. (1), using the time shift property of the FT and appropriate factorization [8–10]

$$\tilde{S}(f) = \frac{\sigma_\epsilon^2}{\left|1 + \sum_{m=1}^{p} a_m \mathrm{e}^{-2\pi i f}\right|^2}, \tag{2}$$

where σ_ϵ^2 is the estimated random input noise variance. The AR's spectra are more reliable than those obtained by FFT because, in using FFT, one assumes that there are an infinity of noiseless experimental data points. Therefore, the resulting spectra are the convolution of the "true" spectra with the observation window. These hypotheses are not assumed in AR estimator and the spectra are obtained using just the data within the recorded time interval.

The value of p, the filter order, is an input parameter. There are several criteria for choosing the optimal value of the filter order [8, 9, 11, 17], The final prediction error (FPE) criterion from Akaike is used in this work [17]. The values of all a_m and σ_ϵ^2 are calculated through the Burg algorithm [18]. A small p renders a spectrum with few broad peaks, in fact the number of peaks is almost equal to $p/2$, since the poles of AR estimator defined as the zeroes of the polynomial are obtained from Eq. (2) by substitution of $z = \mathrm{e}^{2\pi i f}$

$$z^p + a_1 z^{p-1} + \cdots + a_p, \tag{3}$$

a_m values are taken from the denominator of the same equation. The polynomial (3) has p roots with module smaller than unity, lying within the unit circle $|z| < 1$. The angle defined as $\theta = \tan^{-1}(\mathrm{Im}\{z\}/Re\{z\})$ is called the argument of the complex number z and, if $0 \leq \theta \leq \pi$, the complex number is said to belong to the upper half of complex plane. As f, in Eq. (2), varies from 0 to 0.5, $z = \mathrm{e}^{2\pi i f}$ describes the upper half of the unit circle $|z| = 1$. Therefore, the roots of polynomial (3) lying to the upper half of complex plane, also called poles of the AR estimator, determine the spectrum shape. The angle θ is identified as the angular frequency [17]. In our application, a small value for the order parameter provides a better distinction between active and inactive pixels. As remarked, a pixel is classified as active if its time-series spectrum has a peak in the stimulus frequency region. A peak is localized by its pole argument. The module of pole used to classify the pixel as active can be also used to assign the activity intensity. The module closer to unity corresponds to intense peak which indicates more acute stimulus response at that pixel.

2.2 Hemodynamic Response Function

The methods normally used to process the fMRI data assume an "ad hoc" shape for hrf. It is well known that the shape of hrf is difficult to be measured experimentally and in fact it can change form pixel to pixel and temporally. With the proposed method, it is not necessary to do any presupposition.

2.3 Construction of Functional Map

To test the performance of our method, a simulated binary image P (Fig. 1a) was used. The ones and zeroes represent the active and inactive pixel, respectively.

The block paradigm setup was simulated by intercalating three sets of images corresponding to activation periods with three sets of images corresponding to

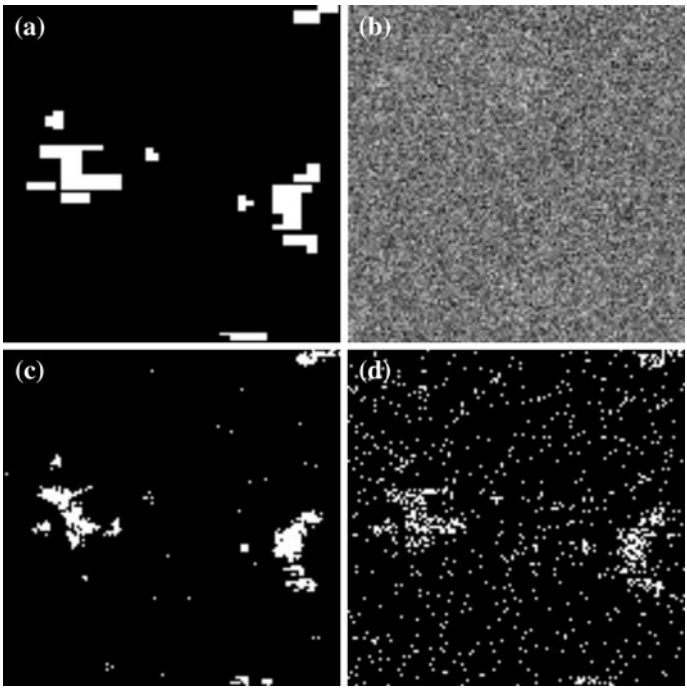

Fig. 1 **a** Simulated functional map used to generate the data. The *white points*, equal to one, represent the active points and the *black ones*, equal to zero, represent the inactive points. **b** One of the 60 slices used to obtain the 128 × 128 time series with 60 points each. It was constructed by adding noise to image **a** (the signal-to-noise ratio is 0.5). **c** Reconstructed functional map using the AR method with the following parameters: AR filter order $p = 20$ and frequencies within $0.267/T_{\mathrm{R}}$ rad/s and $0.361/T_{\mathrm{R}}$ rad/s (stimulus angular frequency ± 15 %), pole intensity equal or great than 0.95 was considered as active pixel. **d** Reconstructed functional map obtained by the Statistical Parametric Mapping Program, significant value of 0.95 was used

resting periods, each set containing ten images (128 × 128 pixels). For each pixel $\boldsymbol{I} = (i, j)$ with $i, j = 1, \ldots, 128$, a time series $Y_{\boldsymbol{I}}(t_n)$ was constructed, where $t_n = nT_{\mathrm{R}}, n = 1, \ldots, 60$. T_{R} represents the time interval between two subsequent images. The $Y_{\boldsymbol{I}}(t_n)$'s were modeled as in [19, 20] considering that (a) the system has an assumed known global hrf [21], that (b) every pixels is either active or not, that (c) at every pixel and time, the MR signal has been corrupted by some noise process, and that (d) linear model, following [22] is adequate:

$$Y_{\boldsymbol{I}}(t_n) = \begin{cases} f_{\boldsymbol{I}}(t_n) + \eta_{\boldsymbol{I}}, & \text{if } P_{\boldsymbol{I}} = 1 \\ \eta_{\boldsymbol{I}}, & \text{if } P_{\boldsymbol{I}} = 0 \end{cases}, \tag{4}$$

where

$$f_{\boldsymbol{I}}(t_n) = b_{\boldsymbol{I}} + A_{\boldsymbol{I}} h(t_n), \tag{5}$$

and $\eta_{\boldsymbol{I}}$ represents the noise process with standard deviation equal to $A/2h_{\boldsymbol{I}}(t_n)$, the hrf is a periodic function with period equal to 20 T_{R}, whose maximum value is 1 (Fig. 2) $A_{\boldsymbol{I}}$ is the signal amplitude, $b_{\boldsymbol{I}}$ is the baseline at the pixel $\boldsymbol{I}$.

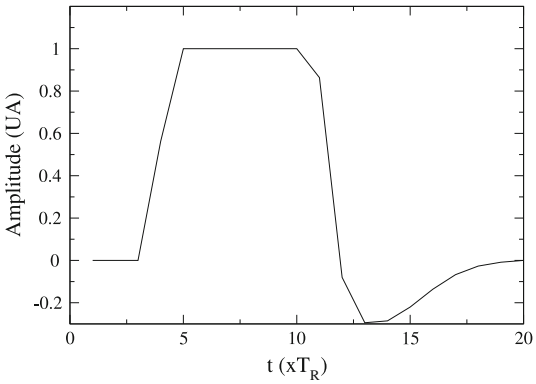

Fig. 2 Hemodynamic response function used in all simulations

3 Results

Instead of applying the AR estimator directly to the sequence $Y_I(t_n)$, given in Eq. (4), it was applied to $Y_I(t_n) - m_I$, where m_I is the mean value of $Y_I(t_n)$ with $\boldsymbol{I}$ constant. In this way, the zero frequency component in the power spectra of Eq. (5) is eliminated. The power spectra of the other signals like the relaxation decay have low frequency and do not interfere with the peak at the stimulus frequency. The "ar.burg" routine from software *R* [23, 24] was used to build a script for the AR method to process the fMRI data. The time series for each pixel was modeled by the AR process with filter order of $p = 20$ and the values of the filter coefficients, a_m, fitted using the Burg's method [8, 11, 18]. Then, the root arguments, θ, of the polynomial (3) gives the peak localization in rad/s units. The pixel is considered as active if its corresponding time series has a root within 2π $(1/T_R \pm 0{,}15/T_R)$ rad/s. The $\pm$ $0.3\pi/T_R$ interval is chosen due to the error induced by phase dependence of Burg's method [25].

The ROC curves were used for quantitative comparison between different methods and different processing parameters. The AR estimator method was compared with the SPM version 8.0 following the tutorial, adapting the corresponding parameters to our simulated data [15]. In all cases, the ROC curve parameter for the AR estimator method was the cutoff value of the pole used to classify the pixel as active. The ROC curve parameter for the SPM was the significance value, labeled as p in the software.

As can be seen in Fig. 3, the present method, solid line, has a better ROC performance if compared with the traditional SPM program [15] (dashed line). For the AR method the filter order was 20 and the roots with the stimulus frequency $\pm$15 % considered as an active pixel. with these conditions and pole cutoff of 0.95, the method result can be seen in Fig. 1c. In Fig. 1d, the SPM result with significant value of 0.95 is shown.

Normally, the AR estimator order parameter is a critical one and should be chosen rather carefully. However, in our case this is not so and p can assume a range of values without influencing drastically the resulting functional map. This can be confirmed quantitatively from the ROC curves obtained for different values

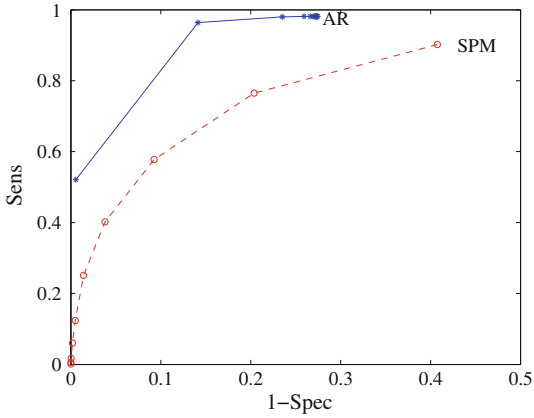

Fig. 3 ROC curves for AR (*solid line*) with filter order of $p = 20$, and for SPM (*dashed line*) [15]. The time series used to build the simulated data had three periods with 20 images by stimulus period and signal-to-noise ratio of 0.5

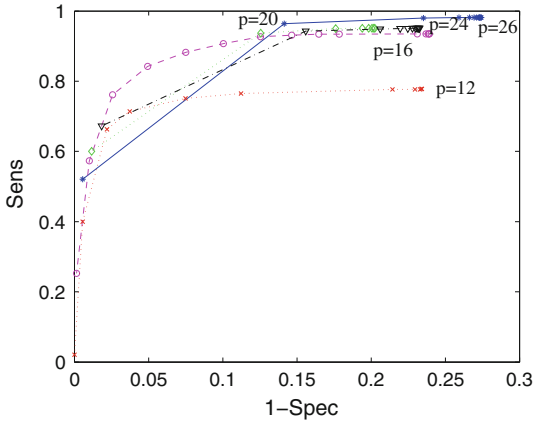

Fig. 4 ROC curves for AR order parameters, $p = 12, 16, 20, 24, 26$. The better ROC curve happens for $p = 20$ (*solid line*)

of p, as it can be seen in Fig. 4, a higher sensitivity and specificity are obtained for $16 \leq p$, curves represented in dashed line ($p = 16$), solid line ($p = 20$), dashed line ($p = 24$) and dotted line ($p = 26$). All those curves have similar behavior. On the other hand, the dotted line ROC curve for $p = 12$ showed a poor performance.

The robustness of the AR method was tested varying the frequency interval used to classify the active/inactive pixels. The interval limits are presented in Table 1.

In Fig. 5, the ROC curve for each interval in Table 1 is shown. The dashed-dotted line, 5 %, has the poor performance as compared to the other intervals. For the solid line, 10 % curve, a higher specificity was achieved and a better sensitivity. For interval with 15 %, dotted curve, a still better sensitivity has reached in relation to the other two cases. For this case, the specificity was decreased. The dashed-dotted curve, 20 % curve, has similar sensitivity as the 15 % case, but, worse specificity.

Another characteristic is the root module distribution, shown in Fig. 6. As it can be seen, the majority of the modulus is concentrated close to zero which

Table 1 Interval limits for angular frequency used to classify active pixels

%	Inferior (rad/s)	Superior (rad/s)
5	0.298	0.330
10	0.28	0.34
15	0.267	0.361
20	0.251	0.377

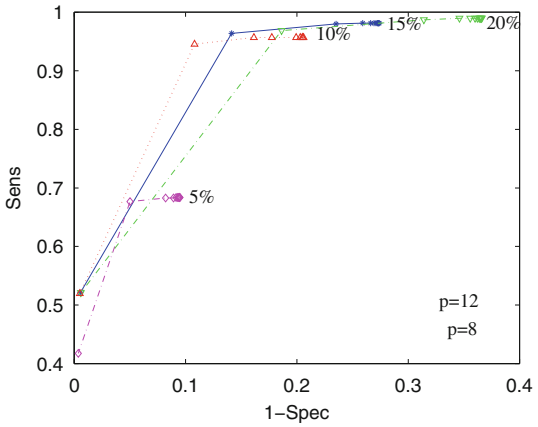

Fig. 5 ROC curves for different frequency intervals

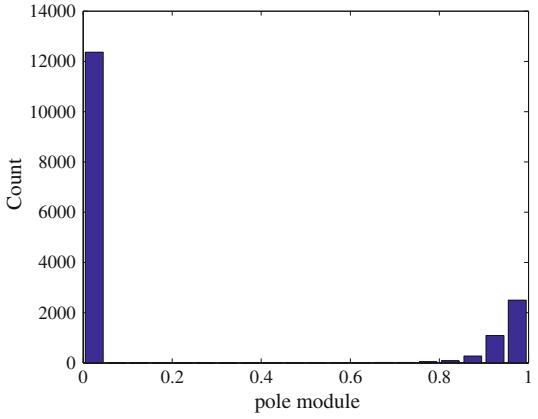

Fig. 6 Histogram for the root polynomial (3) module. The higher count for lower values, zero, correspond to inactive pixels

corresponds to inactive pixels and there is another concentration of modulus close to 1 ($\geq$0.9), corresponding to active pixels.

3.1 Application to Real fMRI Data Set

A bilateral finger tapping experiment was performed in a healthy male subject with 16 s off followed by five epoch of 25 s on and 25 s off, with echo time $T_E = 40$ ms and repetition time $T_R = 3{,}840$ ms. Using a 1.5 T scanner (Siemens, Magneton

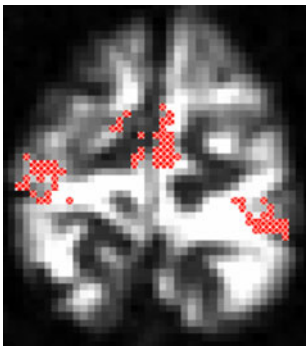

Fig. 7 Result of the application of the AR method in a real fMRI data set (for details see text)

Vision), 64 axial images of a slice passing through the motor cortex were acquired. The 60 final images with a 128 by 128 pixel resolution were used to build the fMRI data set. Figure 7 shows the activity map of the chosen slice obtained by AR method, the active pixels are marked with red crosses. For clarity the result was superimposed on a structural image. The AR filter order was $p = 20$ and a $\pm 15\,\%$ frequency interval was considered.

4 Conclusions

Normally, the frequency of stimulus in block paradigm is precisely known, while the shape and timing of the hemodynamic response is rather ambiguous. The AR estimator analysis, presented in this paper, makes no assumption about the form and timing of the hrf. In fact, it can vary from region to region in brain. The only necessary information is the fact that in block paradigm the stimulus are periodic with known frequency. If the spectrum of the time series corresponding to a pixel contains a peak around the stimulus frequency, it is chosen as active region. The argument of the complex poles of the AR process corresponds to the peaks in the power spectra. In contrary to the FT analysis, the power spectra are obtained without the addition of any "ad hoc" information in to the measured data. This method is easily implemented and computationally it is as fast as other methods. Using the simulated data the AR estimator method was compared to SPM. The comparison between the corresponding ROC curves shows the superiority of the AR estimator.

This method can also be applied to any other fMRI paradigm with periodic stimulus.

Acknowledgments We thank S.D.R. Amaral and N. Caticha, for the simulated fMRI data set, and D. B. Araujo, for the real fMRI data set. This work received the support of FAPESP and CNPq. Script program can be made available by request to hernan@if.usp.br

References

1. S. Ogawa, D.W. Tank, R. Menon, J.M. Ellermann, S.G. Kim, H. Merkle, K. Ugarbil, Proc. Natl. Acad. Sci. USA **89**, 5951 (1992)

2. J.W. Belliveau, D.N. Kennedy, R.C. Mckinstry, B.R. Buchbinder, R.M. Weisskoff, M.S. Cohen, J.M. Vevea, T.J. Brady, B.R. Rosen, Science **254**(5032), 716–719 (1991)
3. K.K. Kwong, J.W. Belliveau, D.A. Chesler, I.E. Goldberg, R.M. Weisskoff, B.P. Poncelet, D.N. Kennedy, B.E.H.M.S. Cohen, R. Turner, H.M. Cheng, J.J. Brady, B.R. Rosen, Proc. Natl. Acad. Sci. USA **89**, 5675 (1992)
4. A.L. Baert, K. Sartor, J.E. Youler, *Funcional MRI* (Springer, New York, 2000)
5. N. Lange, in *Functional MRI*, ed. by C. Moonen, P. Bandettini, Medical Radiology-Diagnostic Imaging and Radiation Oncology, vol. 27 (Springer, New York, 1999), pp. 301–335
6. N. Lange, S.L. Zeger, Appl. Stat. J. Roy. Stat. Soc. Ser. C **46**(1), 1–19 (1997)
7. J.L. Marchini, B.D. Ripley, Neuroimage **12**(4), 366–380 (2000)
8. S. Haykin (ed.), *Nonlinear Methods of Spectral Analysis* (Springer, New York, 1979)
9. P.S. Naidu, *Modern Spectrum Analysis of Time Series* (CRC Press, Boca Raton, 1996)
10. R.D. Brockwell, *Time Series: Theory and Methods* (Springer, New York, 1991)
11. D.M. Lin, E.K. Wong, Phys. Rep. **193**(2), 41–135 (1990)
12. S. Ogawa, D.W. Tank, R. Menon, J.M. Ellermann, S.G. Kim, H. Merkle, K. Ugurbil, Proc. Natl. Acad. Sci. USA **89**(13), 5951–5955 (1992)
13. K.K. Kwong, J.W. Belliveau, D.A. Chesler, I.E. Goldberg, R.M. Weisskoff, B.P. Poncelet, D.N. Kennedy, B.E. Hoppel, M.S. Cohen, R. Turner, H.M. Cheng, T.J. Brady, B.R. Rosen, Proc. Natl. Acad. Sci. USA **89**(12), 5675–5679 (1992)
14. C.T.W. Moonen, P.A. Bandettini, in *Medical Radiology Diagnostic Imaging. Functional MRI*, *volume 27*, ed. by A.L. Baert, K. Sartor, J.E. Youker (Springer, Berlin, 2000)
15. K.J. Friston, J.T. Ashburner, S. Kiebel, T.E. Nichols, W.D. Penny (eds.), *Statistical Parametric Mapping: The Analysis of Functional Brain Images* (Academic Press, New York, 2007)
16. D.B. Rowe, B.R. Logan, Neuroimage **23**(3), 1078–1092 (2004)
17. R.H. Cervantes, S.R. Rabbani, Solid State Commun. **110**(4), 215–220 (1999)
18. J.P. Burg, *A New Analysis Technique for Time Series Data* (NATO, Enschede, 1968)
19. S.D.R. Amaral, S.R. Rabbani, N. Caticha, Neuroimage **23**(2), 654–662 (2004)
20. N. Caticha, S.D. Amaral, S.R. Rabbani, Bayesian Inference Maximum Entropy Methods Sci. Eng. **735**, 27–34 (2004)
21. C. Gossl, L. Fahrmeir, D.P. Auer, Neuroimage **14**(1), 140–148 (2001)
22. K.J. Friston, W. Penny, C. Phillips, S. Kiebel, G. Hinton, J. Ashburner, Neuroimage **16**(2), 465–483 (2002)
23. R. Ihaka, R. Gentleman, R, J. Comput. Graph. Stat. **5**(3), 299–314 (1996). http://www.amstat.org/publications/jcgs/
24. R: Development Core Team, R: a language and environment for statistical computing, R foundation for statistical computing (2010). http://www.R-project.org/
25. W.Y. Chen, G.R. Stegen, J. Geophys. Res. **79**(20), 3019–3022 (1974)